Electron-phonon couplings and carrier mobility in graphynes sheet calculated using the Wannier-interpolation approach

Jinyang Xi, Dong Wang, Yuanping Yi, and Zhigang Shuai

Citation: The Journal of Chemical Physics **141**, 034704 (2014); doi: 10.1063/1.4887538
View online: https://doi.org/10.1063/1.4887538
View Table of Contents: http://aip.scitation.org/toc/jcp/141/3
Published by the American Institute of Physics

Electron-phonon couplings and carrier mobility in graphynes sheet calculated using the Wannier-interpolation approach

Jinyang Xi,[1] Dong Wang,[1] Yuanping Yi,[2] and Zhigang Shuai[1,a)]
[1]*MOE Key Laboratory of Organic OptoElectronics and Molecular Engineering, Department of Chemistry, Tsinghua University, 100084 Beijing, People's Republic of China*
[2]*CAS Key Laboratory of Organic Solids, Institute of Chemistry, Chinese Academy of Sciences, 100190 Beijing, People's Republic of China*

(Received 26 April 2014; accepted 25 June 2014; published online 17 July 2014)

Electron-phonon couplings and charge transport properties of α- and γ-graphyne nanosheets were investigated from first-principles calculations by using the density-functional perturbation theory and the Boltzmann transport equation. Wannier function-based interpolation techniques were applied to obtain the ultra-dense electron-phonon coupling matrix elements. Due to the localization feature in Wannier space, the interpolation based on truncated space is found to be accurate. We demonstrated that the intrinsic electron-phonon scatterings in these two-dimensional carbon materials are dominated by low-energy longitudinal-acoustic phonon scatterings over a wide range of temperatures. In contrast, the high-frequency optical phonons play appreciable roles only at high temperature regimes. The electron mobilities of α- and γ-graphynes are predicted to be $\sim 10^4$ cm^2 V^{-1} s^{-1} at room temperature. © *2014 AIP Publishing LLC*. [http://dx.doi.org/10.1063/1.4887538]

I. INTRODUCTION

Graphene is a two-dimensional (2D) sheet of carbon atoms, which exhibits unusual electronic properties,[1] and has been demonstrated as a promising material for carbon-based electronics.[2–4] The most exciting property of graphene is probably its extremely high carrier mobility at room temperature.[4] There have been growing interests in exploring new graphene-like carbon allotropes in recent years,[5–7] such as graphynes.[8,9] The structure of graphyne is formed by inserting C≡C triple bonds into the honeycomb lattice of graphene, and it takes three typical forms: α-, β-, and γ-graphynes.[10] The electronic structure of α- and β-graphynes features Dirac cones in its Brillouin zone much as in graphene, while γ-graphyne is a semiconductor with a finite band gap. Recently, graphdiyne,[11–13] containing two acetylenic linkages between neighboring benzene rings, has attracted tremendous attention due to the first experimental synthesis.[14] The existence of Dirac cones indicates that the intrinsic carrier mobility of graphyne might be as high as that of graphene. Recent first-principles calculations based on deformation potential approximation predicted that carrier mobilities in both α- and β-graphynes reach $\sim 10^4$ cm^2 V^{-1} s^{-1} at room temperature, and the carrier mobility in 6,6,12-graphyne could be even larger than that in graphene.[15] Not only graphynes with Dirac cones, but also graphdiyne with a bandgap showed excellent transport properties with high electron mobility ($\sim 10^5$ cm^2 V^{-1} s^{-1}) at room temperature.[11]

A key factor in determining the intrinsic carrier mobility of a material is the electron-phonon (e-ph) coupling strength. In our previous studies,[11,15–18] the deformation potential (DP) theory proposed by Bardeen and Shockley[19] was used to describe the e-ph coupling for charge transport, where only the longitudinal-acoustic phonon is considered without any dispersion, and the e-ph coupling matrix is simply expressed by DP constant and the elastic constant. Both parameters can be derived from first-principles by lattice dilation.[16] In graphene, the experimentally derived DP constant lied in a broad range (e.g., 10–50 eV[20–22]), while the various theoretical calculations gave only a few eV (e.g., 2.6 eV,[23] 4.5 eV,[24] 5.14 eV[16]), well below the experiments. Optical phonon scatterings are absent in the DP theory, which have been shown to play an important role in carrier scatterings at room temperature such as in 2D MoS_2.[25] Thus, theoretical analysis of e-ph couplings contributed by different phonon modes with phonon dispersions beyond the DP theory is called for. Borysenko *et al.*[24,26] have studied the e-ph couplings in monolayer and bilayer graphene via first-principles lattice dynamics calculations. It remains a challenge to address the charge carrier scatterings with full consideration of e-ph couplings. Recently, progresses have been made in Wannier-Fourier interpolation method.[27] Computation of e-ph coupling for complex solid becomes possible on fine grids in the first Brillouin zone for both electron and phonon states for large systems, such as naphthalene[28] and K_3-picene.[29]

In the present work, we performed first-principles calculations for electronic structure, phonon bands, e-ph couplings, carrier scattering/relaxation time and mobility in α- and γ-graphynes. For comparison, e-ph couplings in graphene were also calculated for benchmark. In order to obtain the ultra-dense sampling of e-ph coupling matrix elements throughout the Brillouin zone required in charge transport calculations, the Wannier interpolation method[27] was applied and the corresponding accuracy was also examined. The four most important in-plane DP phonon modes: transverse acoustic (TA), longitudinal acoustic (LA), transverse optical (TO), and longitudinal optical (LO) modes were taken into account. We show that the intrinsic charge transport over a wide range of

a)Electronic mail: zgshuai@tsinghua.edu.cn

temperature is dominated by LA phonon scatterings, due to the strongest coupling strength between charge carriers and LA phonons. However, scatterings with optical phonon modes should not be neglected at high temperatures (e.g., 300 K for graphene) or for even low electron energies states (e.g., the electron near the Dirac cone for graphene and α-graphyne). It has been found that the optical phonon scatterings in both α- and γ-graphynes are weaker than those in graphene and can be safely neglected at room temperature. The predicted carrier mobilities of both α- and γ-graphynes are on the order of 10^4 cm^2 V^{-1} s^{-1} at room temperature, which is consistent with DP theory. The lower mobilities of α- and γ-graphynes compared to graphene are due to the stronger LA phonon scatterings of graphynes.

II. METHODOLOGY AND COMPUTATIONAL DETAILS

Density functional perturbation theory (DFPT)[30] is a powerful tool to calculate the vibration properties and e-ph coupling with full consideration of the phonon dispersion and the corresponding normal modes obtained from the first-principles inter-atomic force constants. The key process is to calculate self-consistently the linear variations in both charge density $\Delta\rho(\mathbf{r})$ and Kohn-Sham potential ΔV_{KS} with respect to atomic displacements $\mathbf{u}$ through first-order perturbation for Kohn-Sham equation to give rise to $\frac{\partial\rho}{\partial u}$ and $\frac{\partial V_{KS}}{\partial u}$, starting from $\frac{\partial V_{ion}}{\partial u}$.

The e-ph coupling matrix element for the scattering of an electron in band i at wavevector $\mathbf{k}$ to another state in band j with wavevector $\mathbf{k}+\mathbf{q}$ by a phonon mode λ with wavevector $\mathbf{q}$ is described by

$$g^{\lambda}_{ji}(\mathbf{k},\mathbf{q}) = \sqrt{\frac{\hbar}{2M\omega_{\mathbf{q}\lambda}}}\langle\psi_{j\mathbf{k}+\mathbf{q}}|\Delta_{\mathbf{q}\lambda}V_{KS}|\psi_{i\mathbf{k}}\rangle, \tag{1}$$

where $|\psi_{i\mathbf{k}}\rangle$ and $|\psi_{j\mathbf{k}+\mathbf{q}}\rangle$ are the bare Bloch eigenstates of electron, $\omega_{\mathbf{q}\lambda}$ is the phonon frequency, M is the atomic mass in the unit cell, and $\Delta_{\mathbf{q}\lambda}V_{KS}$ is the derivative of the self-consistent Kohn-Sham potential with respect to the atomic displacement associated with the phonon mode λ and wavevector $\mathbf{q}$.$\Delta_{\mathbf{q}\lambda}V_{KS}$ is explicitly written as[31]

$$\Delta_{\mathbf{q}\lambda}V_{KS} = \sum_{\mathbf{R}}\sum_{s}\frac{\partial V_{KS}}{\partial u_{s\mathbf{R}}}\cdot\frac{\mathbf{e}^{\mathbf{q}\lambda}}{\sqrt{M_s}}\frac{e^{i\mathbf{q}\cdot\mathbf{R}}}{\sqrt{N}}, \tag{2}$$

where $\mathbf{u}_{s\mathbf{R}}$ is the atomic displacement for the sth atom at the lattice vector $\mathbf{R}$, $\mathbf{e}^{\mathbf{q}\lambda}$ is the phonon displacement vector of the λth mode with wavevector $\mathbf{q}$, M_s is the mass of the sth atom, and N is the number of unit cells.

Using the Fermi's golden rule, the e-ph scattering rate for an electron from state $(i, \mathbf{k})$ to $(j, \mathbf{k}+\mathbf{q})$ is given by[32]

$$\begin{aligned}W(i\mathbf{k}\rightarrow j\mathbf{k}+\mathbf{q}) = {}& \frac{2\pi}{\hbar}\left|g^{\lambda}_{ji}(\mathbf{k},\mathbf{q})\right|^2(1-f_{j\mathbf{k}+\mathbf{q}})\\ &\times f_{i\mathbf{k}}[n_{\mathbf{q}\lambda}\delta(\varepsilon_{j\mathbf{k}+\mathbf{q}}-\varepsilon_{i\mathbf{k}}-\hbar\omega_{\mathbf{q}\lambda})\\ &+(1+n_{\mathbf{q}\lambda})\delta(\varepsilon_{j\mathbf{k}+\mathbf{q}}-\varepsilon_{i\mathbf{k}}+\hbar\omega_{\mathbf{q}\lambda})]\end{aligned} \tag{3}$$

where $f_{i\mathbf{k}}$ is the electron distribution and $n_{\mathbf{q}\lambda}$ is the phonon distribution. ϵ is the electron energy. Then the electron distribution variation rate due to e-ph scattering is expressed as[32]

$$\begin{aligned}\frac{\partial f_{i\mathbf{k}}}{\partial t}|_{scatt} = {}& \sum_{\mathbf{q}\lambda j}[W(j\mathbf{k}+\mathbf{q}\rightarrow i\mathbf{k}) - W(i\mathbf{k}\rightarrow j\mathbf{k}+\mathbf{q})]\\ = {}& \frac{2\pi}{\hbar}\sum_{\mathbf{q}\lambda j}\left|g^{\lambda}_{ji}(\mathbf{k},\mathbf{q})\right|^2\{(1-f_{i\mathbf{k}})f_{j\mathbf{k}+\mathbf{q}}[n_{\mathbf{q}\lambda}\delta(\varepsilon_{j\mathbf{k}+\mathbf{q}}\\ &-\varepsilon_{i\mathbf{k}}+\hbar\omega_{\mathbf{q}\lambda})+(1+n_{\mathbf{q}\lambda})\delta(\varepsilon_{j\mathbf{k}+\mathbf{q}}-\varepsilon_{i\mathbf{k}}-\hbar\omega_{\mathbf{q}\lambda})]\\ &-(1-f_{j\mathbf{k}+\mathbf{q}})f_{i\mathbf{k}}[n_{\mathbf{q}\lambda}\delta(\varepsilon_{j\mathbf{k}+\mathbf{q}}-\varepsilon_{i\mathbf{k}}-\hbar\omega_{\mathbf{q}\lambda})\\ &+(1+n_{\mathbf{q}\lambda})\delta(\varepsilon_{j\mathbf{k}+\mathbf{q}}-\varepsilon_{i\mathbf{k}}+\hbar\omega_{\mathbf{q}\lambda})]\}\end{aligned} \tag{4}$$

Under the constant relaxation time approximation: $\frac{\partial f_{i\mathbf{k}}}{\partial t} = -\frac{f_{i\mathbf{k}}-f^0_{i\mathbf{k}}}{\tau_{i\mathbf{k}}}$, where $f^0_{i\mathbf{k}}$ is the electron equilibrium distribution that is Fermi-Dirac distribution, the e-ph scattering relaxation time τ_{k} is given by[32]

$$\begin{aligned}\frac{1}{\tau(i,\mathbf{k})} = {}& \frac{2\pi}{\hbar}\sum_{j\mathbf{q}\lambda}\left|g^{\lambda}_{ji}(\mathbf{k},\mathbf{q})\right|^2\\ &\times\left\{\left[f^0_{j\mathbf{k}+\mathbf{q}}+n^0_{\mathbf{q}\lambda}\right]\delta(\varepsilon_{j\mathbf{k}+\mathbf{q}}-\varepsilon_{i\mathbf{k}}-\hbar\omega_{\mathbf{q}\lambda})\right.\\ &\left.+\left[1+n^0_{\mathbf{q}\lambda}-f^0_{j\mathbf{k}+\mathbf{q}}\right]\delta(\varepsilon_{j\mathbf{k}+\mathbf{q}}-\varepsilon_{i\mathbf{k}}+\hbar\omega_{\mathbf{q}\lambda})\right\}.\end{aligned} \tag{5}$$

Here $n_{\mathbf{q}\lambda} = n^0_{\mathbf{q}\lambda}$, namely, phonon Bose-Einstein distribution. The first and second δ-functions describe the absorption and emission of a phonon $\omega_{\mathbf{q}\lambda}$, respectively. The charge mobility can be obtained by solving the Boltzmann equation in the relaxation time approximation to the first order at the weak electric field.[33] The carrier mobility is expressed as[16]

$$\mu = e\frac{\sum_i\int\tau(i,\mathbf{k})\,v^2(i,\mathbf{k})\frac{\partial f^0_{i\mathbf{k}}}{\partial\varepsilon_{i\mathbf{k}}}d\mathbf{k}}{\sum_i\int f^0_{i\mathbf{k}}d\mathbf{k}}, \tag{6}$$

where $\mathbf{v}(i,\mathbf{k}) = \frac{1}{\hbar}\nabla_{\mathbf{k}}\varepsilon_{i\mathbf{k}}$ is the group velocity of electron.

According to Eqs. (5) and (6), we need to evaluate integrals in $\mathbf{k}$- and $\mathbf{q}$-space overa fine grid for both electrons and phonons with highly accurate e-ph matrix elements. We employed the Wannier-Fourier interpolation method,[27] which was implemented in the following way:

(i) Determining the electronic Hamiltonian $H^{el}_{\mathbf{k}}$, the phonon dynamical matrix $D^{ph}_{\mathbf{q}}$ and the e-ph matrix elements $g(\mathbf{k},\mathbf{q})$ on a coarse grid $N_1^{\mathbf{k}(\mathbf{q})}\times N_2^{\mathbf{k}(\mathbf{q})}\times N_3^{\mathbf{k}(\mathbf{q})}$ points by DFPT.

(ii) The electronic Wannier states are determined by the maximally localized Wannier functions (MLWFs) method,[34]

$$|w_{i\mathbf{R}}\rangle = \frac{1}{\sqrt{N}}\sum_{\mathbf{k}}\left[\sum_j U^{\mathbf{k}}_{ji}|\tilde{\phi}_{j\mathbf{k}}\rangle\right]e^{-i\mathbf{k}\cdot\mathbf{R}}, \tag{7}$$

where N is the number of unit cells, $\mathbf{R}$ is the real-space lattice vector. $|\tilde{\phi}_{j\mathbf{k}}\rangle$ is a smooth Bloch eigenstate, defined

by projection,[35]

$$|\tilde{\phi}_{i\mathbf{k}}\rangle = \sum_{j=1}^{J} |\phi_{j\mathbf{k}}\rangle (S_{\mathbf{k}}^{-1/2})_{ji}, \tag{8}$$

where $|\phi_{i\mathbf{k}}\rangle = \sum_{j=1}^{J_k} |\psi_{j\mathbf{k}}\rangle\langle\psi_{j\mathbf{k}}|g_i\rangle$, $(S_{\mathbf{k}})_{ji} = \langle\phi_{j\mathbf{k}}|\phi_{i\mathbf{k}}\rangle$. $|\psi_{j\mathbf{k}}\rangle$ is the Bloch eigenstate calculated from DFT directly. $g_i(\mathbf{r})$ is a set of J localized initial guess of WFs, such as s, p or hybrid orbitals. For isolated bands, $J_{\mathbf{k}}$ at each $\mathbf{k}$ equal to the number of WFs J. However, because of the overlap and hybridization between bands, $J_{\mathbf{k}}$ could be larger than the preset J because the bands are entangled within a defined energy window and the overlap $\langle\psi_{j\mathbf{k}}|g_i\rangle$ becomes a rectangular $J_{\mathbf{k}} \times J$ matrix. In some cases, the energy bands of this projection do not correspond to any of the original energy bands due to the mixing between electronic states. In order to preserve the properties of a system within a given energy range, the frozen energy window is defined. The electronic states lying within the frozen energy window are kept unchanged in the projection step. The details for the projection can be referred to Ref. 35.

Then, the unitary gauge matrix $U_{ji}^{\mathbf{k}}$ in Eq. (7) can be determined by minimizing the mean squared spread of the WFs,

$$\Omega = \sum_i [\langle w_{i\mathbf{0}}|\mathbf{r}^2|w_{i\mathbf{0}}\rangle - \langle w_{i\mathbf{0}}|\mathbf{r}|w_{i\mathbf{0}}\rangle^2]. \tag{9}$$

Once $\{U_{\mathbf{k}}\}$ and the eigenvectors of the phonon dynamical matrix $\{\mathbf{e}_{\mathbf{q}}\}$ are obtained on the coarse grid (the band index i and the phonon mode index λ are omitted for clarity), the electronic Hamiltonian, the phonon dynamical matrix and the e-ph matrix elements in the real space can be described as[27]

$$H^{el}_{\mathbf{R}_e,\mathbf{R}'_e} = \sum_{\mathbf{k}} e^{-i\mathbf{k}\cdot(\mathbf{R}'_e-\mathbf{R}_e)} U^{+}_{\mathbf{k}} H^{el}_{\mathbf{k}} U_{\mathbf{k}}, \tag{10}$$

$$D^{ph}_{\mathbf{R}_p,\mathbf{R}'_p} = \sum_{\mathbf{q}} e^{-i\mathbf{q}\cdot(\mathbf{R}'_p-\mathbf{R}_p)} \mathbf{e}_{\mathbf{q}} D^{ph}_{\mathbf{q}} \mathbf{e}^{+}_{\mathbf{q}}, \tag{11}$$

$$g(\mathbf{R}_e, \mathbf{R}_{\mathrm{p}}) = \frac{1}{N_{\mathrm{p}}} \sum_{\mathbf{k},\mathbf{q}} e^{-i(\mathbf{k}\cdot\mathbf{R}_e+\mathbf{q}\cdot\mathbf{R}_p)} U^{+}_{\mathbf{k}+\mathbf{q}} g(\mathbf{k},\mathbf{q}) U_{\mathbf{k}} \mathbf{e}^{-1}_{\mathbf{q}}, \tag{12}$$

where $\mathbf{R}_{\mathrm{e}}$ and $\mathbf{R}_{\mathrm{p}}$ are the position of the unit cell for describing electron and phonon in real space, respectively. For $\mathbf{k}(\mathbf{q})$-grid $N_1^{\mathbf{k}(\mathbf{q})} \times N_2^{\mathbf{k}(\mathbf{q})} \times N_3^{\mathbf{k}(\mathbf{q})}$ in reciprocal space, there are $N_{k(\mathbf{q})} = N_1^{\mathbf{k}(\mathbf{q})} \times N_2^{\mathbf{k}(\mathbf{q})} \times N_3^{\mathbf{k}(\mathbf{q})}$ unit cells in real space. The number of $N_{\mathbf{k}}$ and $N_{\mathbf{q}}$ can be different, so $\mathbf{R}_{\mathrm{e}}$ and $\mathbf{R}_{\mathrm{p}}$ can also be different. The electronic Hamiltonian matrix elements in real space $H^{el}_{\mathbf{R}_e,\mathbf{R}'_e}$ decay with the distance $|\mathbf{R}_e - \mathbf{R}'_e|$. The spatial decay is determined by the localization of the electronic WFs. However, the localization of phonon dynamical matrix $D^{ph}_{\mathbf{R}_p,\mathbf{R}'_p}$ depends on the dielectric screening, instead of the overlap of lattice WFs centered in the unit cells $\mathbf{R} = \mathbf{R}_{\mathrm{p}}$ and $\mathbf{R} = \mathbf{R}'_{\mathrm{p}}$. The e-ph matrix elements vanish whenever $\mathbf{R}_e$ or $\mathbf{R}_{\mathrm{p}}$ corresponding to a unit cell sufficiently distant from the origin of the reference frame, because of the localization of both $H^{el}_{\mathbf{R}_e,\mathbf{R}'_e}$ and $D^{ph}_{\mathbf{R}_p,\mathbf{R}'_p}$ in real space. Thus, we only need to know a small number of quantities in real space.

(iii) The next step is the transformation from the real space to the reciprocal space on the fine Brillouin zone grid. The Hamiltonian, the phonon dynamical matrix, and the e-ph matrix elements on the fine grid with $N_1'^{\mathbf{k}(\mathbf{q})} \times N_2'^{\mathbf{k}(\mathbf{q})} \times N_3'^{\mathbf{k}(\mathbf{q})}$ points can be expressed as

$$H^{el}_{\mathbf{k}'} = U_{\mathbf{k}'} \left(\frac{1}{N_e} \sum_{\mathbf{R}_e} e^{i\mathbf{k}'\cdot\mathbf{R}_e} H^{el}_{\mathbf{0},\mathbf{R}_e} \right) U^{+}_{\mathbf{k}'}, \tag{13}$$

$$D^{ph}_{\mathbf{q}'} = \mathbf{e}^{+}_{\mathbf{q}'} \left(\frac{1}{N_{\mathrm{p}}} \sum_{\mathbf{R}_{\mathrm{p}}} e^{i\mathbf{q}'\cdot\mathbf{R}_{\mathrm{p}}} D^{ph}_{\mathbf{0},\mathbf{R}_{\mathrm{p}}} \right) \mathbf{e}_{\mathbf{q}'}, \tag{14}$$

$$g(\mathbf{k}', \mathbf{q}') = \frac{1}{N_e} \sum_{\mathbf{R}_e,\mathbf{R}_p} e^{i(\mathbf{k}'\cdot\mathbf{R}_e+\mathbf{q}'\cdot\mathbf{R}_p)} U_{\mathbf{k}'+\mathbf{q}'} g(\mathbf{R}_e, \mathbf{R}_{\mathrm{p}}) U^{+}_{\mathbf{k}'} \mathbf{e}. \tag{15}$$

The summations are truncated outside of a real space supercell containing $N_{\mathbf{k}(\mathbf{q})}$ unit cells. By diagonalizing the terms within the brackets in Eqs. (13) and (14) at fixed $\mathbf{k}'$, and $\mathbf{q}'$, one can obtain the new e-ph matrix element $g(\mathbf{k}', \mathbf{q}')$ according to Eq. (15). A suitable size of coarse Brillouin zone grid and examine the spatial localization of $H^{el}_{\mathbf{R}_e,\mathbf{R}'_e}$, $D^{ph}_{\mathbf{R}_p,\mathbf{R}'_p}$, $g(\mathbf{R}_e, \mathbf{R}_{\mathrm{p}})$.

All the electronic structure and phonon dispersion calculations were performed based on the DFT and DFPT[30] as implemented in the QUANTUM-ESPRESSO package.[36] We used a plane wave basis set, ultrasoft pseudopotential, and Perdew-Burke-Ernzerhof (PBE)[36] generalized gradient approximation (GGA) exchange-correlation functional. The plane wave cutoff was 60 Ry for wavefunctions and 600 Ry for the charge density. The interlayer distance was set to be as large as 15 Å in order to eliminate interlayer interaction. For structural optimizations and electronic structure calculations, the momentum space was sampled on a 36 × 36 × 1 Monkhorst-Pack[37] grid for graphene and 18 × 18 × 1 grid for both α- and γ-graphynes. The Hellmann-Feynman force components on each atom were relaxed to less than 0.0001 Ry/bohr.

The e-ph coupling calculations were carried out by the Wannier interpolation method as implemented in the EPW code.[38] The electronic Wannier states were determined by MLWFs with the WANNIER90 code.[39] To obtain the electron Hamiltonian in MLWFs representations, the in-plane bonding WFs, p_z-like WFs (one per carbon atom) and two s-like WFs located above and below the center of the hexagons in the unit cell of these systems were used for the initial guess. These WFs contained the electronic states below and around the Fermi level. A maximum frozen window of 5.6 eV for graphene, 4.84 eV for α-graphyne and 2.48 eV for γ-graphyne up the Fermi level was chosen to localize the WFs, respectively. For the e-ph matrix elements in these three carbon materials, electronic and phonon states were first

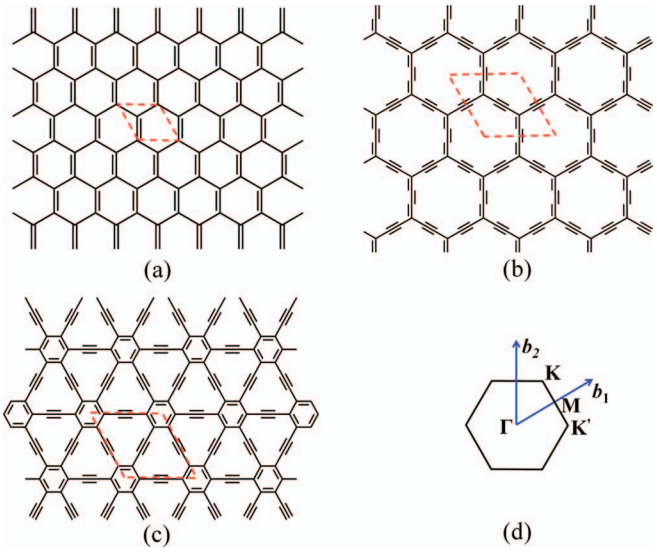

FIG. 1. Structures of (a) graphene, (b) α-graphyne, and (c) γ-graphyne. The dashed red rhombus indicates the unit cell. (d) The first Brillouin zone of the unit cell with four high symmetry points. The lines $\boldsymbol{b}_1$ and $\boldsymbol{b}_2$ are the reciprocal lattice vectors.

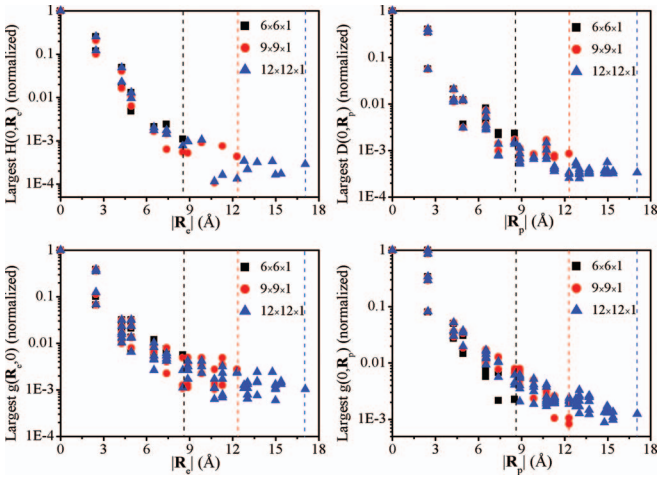

FIG. 2. Spatial decay of the largest components of (a) the Hamiltonian $H^{el}_{\mathbf{R}_e,\mathbf{0}}$, (b) the dynamical matrix $D^{ph}_{\mathbf{R}_p,\mathbf{0}}$, (c) the e-ph coupling matrix elements $g_{\mathbf{R}_e,\mathbf{0}}$ and (d) $g_{\mathbf{0},\mathbf{R}_p}$ with different truncate grids for graphene. The data are normalized to their largest value. The dashed lines denote the truncate distances $|\mathbf{R}|$ corresponding to three coarse $\mathbf{k}(\mathbf{q})$-grids ($6 \times 6 \times 1$, $9 \times 9 \times 1$, $12 \times 12 \times 1$), respectively.

calculated on a coarse $6 \times 6 \times 1$ **k**- and **q**-grids. The interpolated fine **k**- and **q**-grid in transport property calculations was $120 \times 120 \times 1$ for graphene, and $80 \times 80 \times 1$ for α- and γ-graphynes (the **k**- and **q**-grids are used the same size in present work).

III. RESULTS AND DISCUSSION

A. The accuracy of Wannier-interpolation, taking graphene as an example

In order to check the localization of electronic Hamiltonian, the phonon dynamical matrix and e-ph matrix elements in the real space and the corresponding accuracy of the interpolated values in the reciprocal space, we examined these physical quantities for graphene interpolated on three different coarse $\mathbf{k}(\mathbf{q})$-grids ($6 \times 6 \times 1$, $9 \times 9 \times 1$, $12 \times 12 \times 1$). The structure of graphene is shown in Fig. 1(a) with the optimized lattice constant 2.462 Å. Typically MLWFs are localized within a few Å.[40,41] The spreads of WFs defined by Eq. (9) with different truncations are less than 2 Å^2, as shown in Table I. The spatial decay of the largest components of electronic Hamiltonian, the phonon dynamical matrix and the e-ph matrix elements in the real space with different truncate grids are illustrated in Fig. 2. It is found that these physical quantities exponential decay with the distance $|\mathbf{R}|$ between unit cells and thus all the three truncate distances are enough.

TABLE I. The spreads of three types of WFs in Å^2 for graphene on three different $\mathbf{k}(\mathbf{q})$-grids: $6 \times 6 \times 1$, $9 \times 9 \times 1$, and $12 \times 12 \times 1$, respectively.

Type of WFs	$6 \times 6 \times 1$	$9 \times 9 \times 1$	$12 \times 12 \times 1$
in-plane bonding WFs	0.580	0.595	0.600
p_z-like WFs	0.878	0.903	0.909
s-like WFs	1.431	1.551	1.633

To further examine the accuracy, we depict the electronic band structure and phonon dispersion along the high symmetry lines with different truncations in Fig. 3. The band structures below the frozen window are well reproduced with Wannier interpolation when compared with the result from DFT calculation for each coarse **k**-grid. The phonon dispersions from interpolation of different coarse **q**-grids are exactly the same to each other and well matched the results of DFT. We should note that the localization of phonon dynamical matrix is due to effectiveness of the dielectric screening in the material, which is different to the localization of the electronic WFs. Since at $\mathbf{k} = \mathbf{K}$ (Dirac point) the electronic states are doubly degenerate for graphene, we define the square of e-ph coupling matrix element averaged over the Fermi

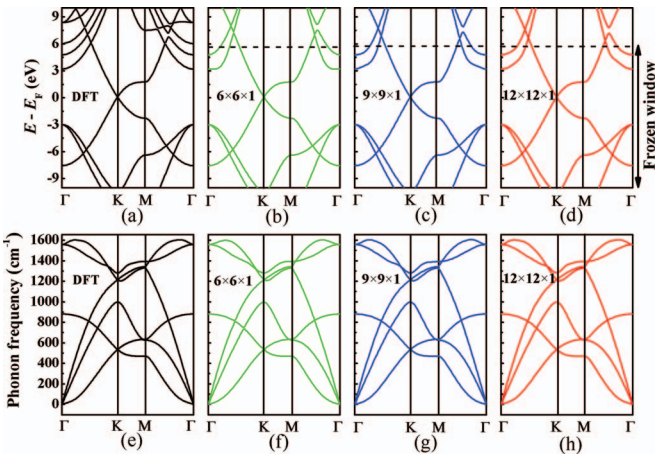

FIG. 3. The band structures and phonon dispersions for graphene along the high symmetry lines by (a), (e) DFT calculations and Wannier-interpolations on (b), (f) $6 \times 6 \times 1$, (c), (g) $9 \times 9 \times 1$, (d), (h) $12 \times 12 \times 1$ coarse $\mathbf{k}(\mathbf{q})$-grids, respectively. The dashed lines show the maximum frozen window to localize the WFs.

surface as[42,43] $\langle g^2_{\mathbf{q}}\rangle_F = \sum_{i,j\in\pi,\pi^*} |g_{j\mathbf{K}+\mathbf{q},i\mathbf{K}}|^2/4$ with LO phonon $\mathbf{q} = \mathbf{\Gamma}$ or $\mathbf{K}$, where the sum is performed over the two degenerate π and π^* bands at the Dirac cone. The factor of 4 in the denominator stems from four possible scattering channels for graphene at the Fermi surface: intraband ($\pi\to\pi$, $\pi^*\to\pi^*$) and interband ($\pi\to\pi^*$, $\pi^*\to\pi$). It is found that the e-ph coupling matrix elements are almost the same for three different truncations with $\langle g^2_\Gamma\rangle_F = 0.0405\, eV^2$, $\langle g^2_K\rangle_F = 0.1$ eV^2 and are in good agreement with other results (0.0401 eV^2,[42] 0.0405 eV^2 [43] for $\mathbf{q} = \mathbf{\Gamma}$; 0.0986 eV^2,[42] 0.0994 eV^2[43] for $\mathbf{q} = \mathbf{K}$). In conclusion, the electronic Hamiltonian, the phonon dynamical matrix, and e-ph matrix elements are localized in the real space for different truncations and the corresponding electronic band structure, phonon dispersion, and e-ph coupling matrix elements are in good agreement with the results from DFT calculations without truncation. The Wannier-interpolation method are reliable and the results interpolated on the coarse $\mathbf{k}(\mathbf{q})$-grid 6 × 6 × 1 for graphene are chosen in the following discussions.

B. The electronic structure, phonon dispersion, and corresponding localization for α-graphyne and γ-graphyne

The structures of α-graphyne and γ-graphyne are illustrated in Figs. 1(b) and 1(c). The optimized lattice constants are 6.987 Å for α-graphyne and 6.883 Å for γ-graphyne, respectively. These results are in good agreement with previous GGA calculations (6.981 Å for α-graphyne and 6.883 Å for γ-graphyne;[9] 6.889 Å for γ-graphyne[44]). The calculated spreads of WFs in these systems are typically around 1 Å^2, see Table II, namely, very localized.

The band structures of α-graphyne and γ-graphyne are depicted in Figs. 4(a) and 4(b). The black-solid lines and red scatters stand for the electronic bands calculated without and with Wannier interpolations, respectively. Within the maximum frozen window, the agreement is perfect. It indicates good localization of the WFs. For α-graphyne, two Dirac cones locate at $\mathbf{K}$- and $\mathbf{K}'$-points of the first Brillouin zone, similar to graphene. By linearly fitting the π and π^* band energies near $\mathbf{k} = \mathbf{K} + \mathbf{k}'$ to the expression $E(|\mathbf{k}'|) = \hbar v_F|\mathbf{k}'|$, we obtained the Fermi velocity of α-graphyne to be 0.75 × 10^6 m/s, consistent with previous DFT calculations.[9,45]

Different from graphene, the bonds in α-graphyne originate from different types, both sp^2 and sp^1 carbon hybridizations, and the large carbon rings in α-graphyne leads to weaker σ bonding. Figs. 5(a) and 5(b) plot the charge density distribution near the Fermi level of graphene and α-graphyne, respectively. It is found that the π (π^*) bonding between neighbouring carbon atoms in α-graphyne is weaker

TABLE II. The convergent average and largest spreads of WFs in Å^2 for graphene, α-graphyne, and γ-graphyne.

	Graphene	α-graphyne	γ-graphyne
Average spread	0.908	0.854	0.916
Largest spread	1.431	1.013	1.022

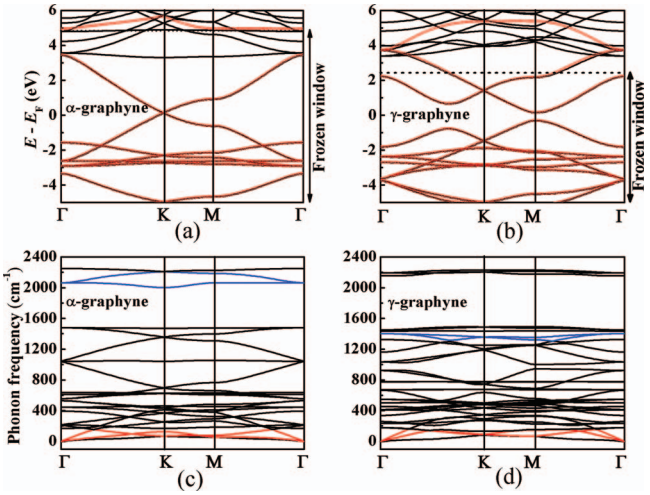

FIG. 4. Band structures and phonon dispersions of (a), (c) α-graphyne and (b), (d) γ-graphyne, respectively. The dispersion is along the high symmetry lines. The black-solid lines and red scatters stand for the results from direct DFT calculations and Wannier interpolations on 6 × 6 × 1 coarse $\mathbf{k}(\mathbf{q})$-grids, respectively. The dotted lines show the maximum frozen window to localize the WFs. In (c) and (d), the blue and red lines stand for the special optical modes (upper is LO, lower is TO) and acoustic modes (upper is LA, lower is TA), respectively.

than that of graphene, leading to narrower band width and smaller Fermi velocity. As will be discussed below, these bonding characteristics significantly affect e-ph coupling in α-graphyne. Different from graphene and α-graphyne, a direct bandgap of 0.454 eV at the $\mathbf{M}$-point is found in γ-graphyne, which is consistent with others' studies.[46,47] The phonon dispersion relations, shown in Figs. 4(c) and 4(d), can be derived once the phonon dynamical matrix is obtained from the DFPT. The phonon frequencies in the dispersion curves are all positive, indicating the structure stability. The three lowest modes are the acoustic phonon modes and the other 3n-3 (n is the number of atoms in the unit cell) modes are all optical phonon modes. The acoustic modes include in-plane and out-of-plane atomic displacements along the Cartesian axes, and the optical modes display the atomic displacements with bond-bending and bond-stretching characters. In graphene and α-graphyne, the Kohn anomaly[48] is observed at the $\mathbf{\Gamma}$- and $\mathbf{K}$-points (near 1558 cm^{-1} and 1281 cm^{-1}

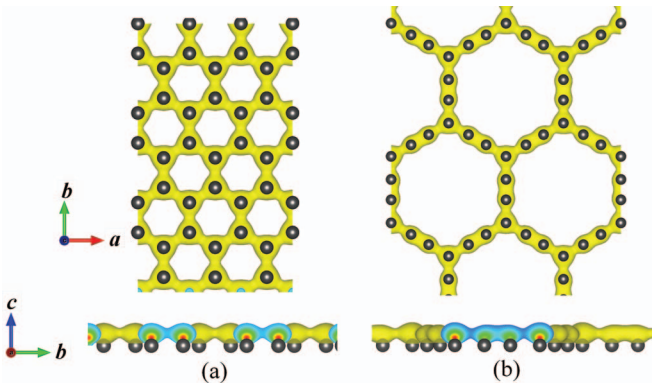

FIG. 5. Band-decomposed charge density distribution of the π (π^*) bands near the Fermi level of (a) graphene and (b) α-graphyne from both top (upper) and side (lower) views. The isovalue is 1.815 × 10^{-4} eÅ^{-3}.

TABLE III. Phonon energies in meV for LA, TA, LO and TO modes at the **Γ**, **K**, and **M** points in the first Brillouin zone of graphene, α-graphyne, and γ-graphyne.

	Graphene			α-graphyne			γ-graphyne		
Phonon mode	**Γ**	**K**	**M**	**Γ**	**K**	**M**	**Γ**	**K**	**M**
LA	0.0	123.6	78.8	0.0	15.6	9.7	0.0	11.2	17.9
TA	0.0	66.3	77.6	0.0	8.4	7.2	0.0	11.2	8.4
LO	193.2	158.8	172.6	255.8	273.9	271.1	173.8	168.3	167.8
TO	193.2	150.7	166.4	255.8	248.1	255.7	173.8	168.3	163.8

for graphene, 2063 cm^{-1} and 2001 cm^{-1} for α-graphyne, as shown in Figs. 3(e) and 4(c), respectively) arising from the strong e-ph coupling with optical phonon modes, which will be discussed in Sec. III C. In the present study, we focus on e-ph couplings with four in-plane DP phonon modes, which include: TA, LA, TO (E_{2g} symmetry) as well as LO (E_{2g}). The e-ph couplings to other phonon modes are insignificant from our calculations, and are not discussed in this work. In Figs. 4(c) and 4(d), the blue and red lines along high symmetry directions stand for the special optical modes (upper is LO, lower is TO) and acoustic modes (upper is LA, lower is TA) in α- and γ-graphynes, respectively. The phonon energies of LA, TA, LO, and TO modes at different symmetry points are summarized in Table III.

To further investigate the localization of the Hamiltonian, the dynamical matrix, and the e-ph coupling matrix in real space for graphyne, we depict in Fig. 6 the spatial decay of the largest components of the corresponding physical quantities as a function of the inter unit cell distance, taking α-graphyne as an example. It is found that the decay is indeed exponential. The similar behavior is found for γ-graphyne. It is found that the decay is indeed exponential. As a consequence, we only need to keep a small number of these physical quantities for Wannier-interpolation. In the present work, these physical quantities were truncated within a real space supercell containing $N_{\mathbf{k(q)}} = 36$ unit cells for both electrons and phonons. The corresponding truncation distance $|\mathbf{R}| = |\mathbf{R}_{e(p)}–\mathbf{R}_0|$ for matrix elements is about 24.07 Å for α-graphyne and 23.81 Å for γ-graphyne, respectively.

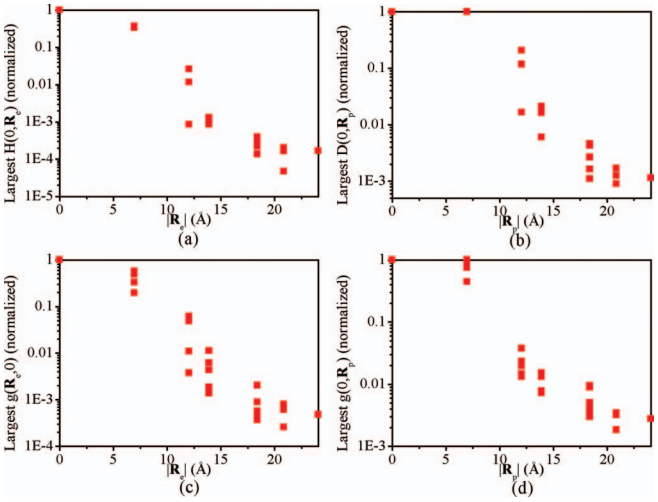

FIG. 6. Spatial decay of the largest components of (a) the Hamiltonian $H^{el}_{\mathbf{R}_e,0}$, (b) the dynamical matrix $D^{ph}_{\mathbf{R}_p,0}$, (c) the e-ph coupling matrix elements $g_{\mathbf{R}_e,0}$ and (d) $g_{0,\mathbf{R}_p}$ for α-graphyne as a function of distance. The data are normalized to their largest value and are taken along several directions.

C. Electron-phonon couplings and deformation potential

Now, following the calculations in truncated real space, the Hamiltonian, dynamical matrix, and e-ph coupling matrix are Fourier transformed back to the reciprocal space on extremely fine Brillouin zone grids. We first compare the square of the e-ph coupling matrix elements for the optical phonon modes in α-graphyne with those in graphene as defined in Sec. III A. The results are summarized in Table IV. In α-graphyne, $\langle g^2_\Gamma\rangle_F = 0.0128\,eV^2$(scattered by LO mode) and $\langle g^2_\mathbf{K}\rangle_F = 0.027\ eV^2$ (scattered by TO mode) are about 70% smaller than those in graphene (0.0405 eV^2 at $\mathbf{q} = \mathbf{\Gamma}$ and 0.1003 eV^2 at $\mathbf{q} = \mathbf{K}$, respectively).

The smaller e-ph coupling matrix elements in α-graphyne indicate the weaker Kohn anomaly, as can be seen from the phonon dispersions for optical modes at $\mathrm{q} = \mathbf{\Gamma}$ and **K** in Fig. 7. An interesting finding is that in both graphene and α-graphyne, the ratio $\langle g^2_\mathbf{K}\rangle_F\omega_\mathbf{K}/\langle g^2_\Gamma\rangle_F\omega_\Gamma$ is close to the value of 2.0, which is similar to the case in 2D silicene and germanene.[49]

Figs. 8(a)–8(c) depict the square of e-ph coupling matrix elements in Eq. (1) as a function of the LA phonon wavevector **q** (near the center of Brillouin zone) for graphene, α-graphyne, and γ-graphyne, respectively. The electronic states (both initial and final states for e-ph scatterings) are limited to the conduction band (CB) (the electronic wavevector **k** is in the **K**-valley for graphene and α-graphyne, in the **M**-valley for γ-graphyne). The scattering matrix elements manifest clear isotropy near the center of Brillouin zone. In DP theory, for

TABLE IV. Phonon frequencies ω (in cm^{-1}) and $\langle g^2_\mathrm{q}\rangle_F$ (in eV^2) at **Γ**- and **K**-points for LO mode in graphene, for LO mode at **Γ** and TO mode at **K** in α-graphyne.

		q at **Γ**		**q** at **K**		
		ω	$\langle g^2_\mathbf{K}\rangle_F$	ω	$\langle g^2_\mathbf{K}\rangle_F$	$\frac{\langle g^2_\mathbf{K}\rangle_F\omega_\mathbf{K}}{\langle g^2_\Gamma\rangle_F\omega_\Gamma}$
Graphene	Ref. 43	1540	0.0405	1250	0.0994	1.98
	Ref. 42	1586	0.0401	1320	0.0986	2.05
	This work	1558	0.0405	1281	0.1003	2.04
α-graphyne	This work	2063	0.0128	2001	0.0270	2.04

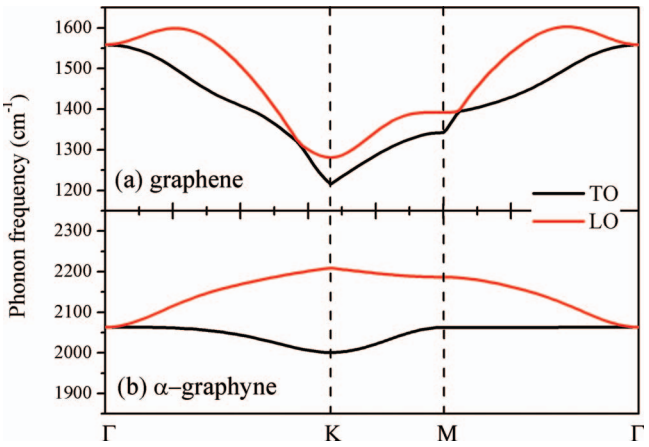

FIG. 7. The phonon dispersions of LO and TO modes along the high symmetry lines for (a) graphene and (b) α-graphyne, respectively. The red lines stand for LO mode and the black lines stand for TO mode.

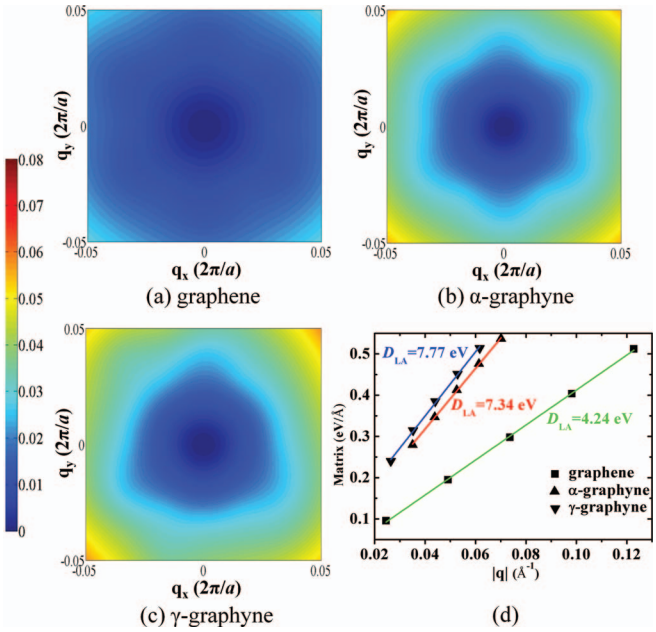

FIG. 8. Contour plots showing the square of e-ph coupling matrix elements $|g^{\lambda}_{ji}(\mathbf{k},\mathbf{q})|^2$ (in eV^2) calculated by Wannier-interpolation for (a) graphene, (b) α-graphyne, and (c) γ-graphyne, as a function of LA phonon wavevector $\mathbf{q}$ (near the center of the Brillouin zone). $\mathbf{k}$ is at the CB minimum (**K**-point for graphene and α-graphyne, **M**-point for γ-graphyne) and the initial i and final j electron states are both limited to CB. (d) The matrix element of LA phonon scattering as a function of phonon wavevector $\mathbf{q}$ in the long-wavelength limit. The slope is the first-order LA DP constant. The solid lines are the fitting curves. The block represents graphene, the circle represents α-graphyne and the down-triangle γ-graphyne.

scattering with acoustic phonons in the long-wavelength limit, the matrix element is linear in $|\mathbf{q}|$:[50]

$$M^{\lambda}_{ii}(\mathbf{k},\mathbf{q}) = \langle i,\mathbf{k}+\mathbf{q}|\delta_{\mathbf{q}\lambda}V_{SCF}|i,\mathbf{k}\rangle = D^{1}_{\lambda}|\mathbf{q}|, \qquad (16)$$

where D^{1}_{λ} is the first-order acoustic DP constant. According to Eq. (16), the LA DP constants of graphene, α-graphyne, and γ-graphyne are obtained by a linear fitting of the matrix element at $|\mathbf{q}| \to 0$, as shown in Fig. 8(d). It is found that the LA DP constant of graphene is 4.24 eV, close to others' first-principles calculations of the effective acoustic DP constants (e.g., 4.5 eV by direct lattice dynamics calculations,[24] 6.8 eV by the group theoretical considerations[51]). This value is also in agreement with the result (5.14 eV[16]) obtained within the DP theory, by linear fitting of the band edge shift with respect to the unit cell dilation. The LA DP constants for α-graphyne (7.34 eV) and γ-graphyne (7.77 eV) are larger than that of graphene, suggesting stronger LA phonon scattering in α- and γ-graphynes.

Different from intra-valley acoustic phonon scattering, the optical phonon scattering and inter-valley acoustic phonon scattering are treated by the zeroth-order DP theory[50]

$$M^{\lambda}_{ii}(\mathbf{k},\mathbf{q}) = \langle i,\mathbf{k}+\mathbf{q}|\,\delta_{\mathbf{q}\lambda}V_{SCF}\,|i,\mathbf{k}\rangle = D^{0}_{\lambda}, \qquad (17)$$

where D^{0}_{λ} is the zeroth-order acoustic or optical DP constant. Based on the Wannier interpolation evaluated e-ph coupling matrix elements and Eqs. (16) and (17), the LA, TA, LO, and TO DP constants of graphene, α-graphyne, and γ-graphyne are summarized in Table V. The DP constants of intra-valley phonon scattering (i.e., **M**→**M**) in γ-graphyne show that the main scattering modes are LA, LO, and TO. For graphene and α-graphyne, due to the valley degeneracy, the DP constants of both intra-valley scattering (i.e., **K**→ **K** by LA, TA, LO, and TO) and inter-valley scattering (i.e., **K**→ K' by LA, TA, LO, and TO) are considered. It is found that the main scattering modes in both graphene and α-graphyne are intra-valley LA, intra-valley LO, as well as inter-valley optical modes. The optical phonon DP constants in graphene are larger than those in α-graphyne (e.g., $D^{0}_{LO,\mathbf{KK}}$ is 3.78×10^8 eV/cm for graphene and 1.73×10^8 eV/cm for α-graphyne),

TABLE V. DP constants extracted for e-ph coupling in graphene, α-graphyne, and γ-graphyne for the electronic states (both initial and final) limited to the CB minimum (**K**-valley for graphene and α-graphyne, **M**-valley for γ-graphyne). The symbol of N/A means no value output due to too small e-ph coupling. Especially, only intra-valley DP is considered for γ-graphyne.

Phonon mode		Graphene	α-graphyne	γ-graphyne
Intra-valley	LA	$D^{1}_{\mathrm{LA},\mathbf{KK}} = 4.24$ eV	$D^{1}_{\mathrm{LA},\mathbf{KK}} = 7.34$ eV	$D^{1}_{\mathrm{LA},\mathbf{MM}} = 7.77$ eV
Acoustic	TA	$D^{1}_{\mathrm{TA},\mathbf{KK}} = 1.70$ eV	N/A	N/A
Inter-valley	LA	N/A	$D^{0}_{\mathrm{LA},\mathbf{KK}'} = 7.65\times10^3$ eV/cm	...
Acoustic	TA	$D^{0}_{\mathrm{TA},\mathbf{KK}'} = 4.43 \times 10^3$ eV/cm	$D^{0}_{\mathrm{TA},\mathbf{KK}'} = 3.00 \times 10^5$ eV/cm	...
Intra-valley	LO	$D^{0}_{\mathrm{L0},\mathbf{KK}} = 3.78 \times 10^8$ eV/cm	$D^{0}_{\mathrm{L0},\mathbf{KK}} = 1.73 \times 10^8$ eV/cm	$D^{0}_{\mathrm{L0},\mathbf{MM}} = 1.01 \times 10^8$ eV/cm
Optical	TO	N/A	$D^{0}_{\mathrm{T0},\mathbf{KK}} = 4.69 \times 10^7$ eV/cm	$D^{0}_{\mathrm{T0},\mathbf{MM}} = 1.17\times10^8$ eV/cm
Inter-valley	LO	$D^{0}_{\mathrm{L0},\mathbf{KK}'} = 5.40 \times 10^8$ eV/cm	$D^{0}_{\mathrm{L0},\mathbf{KK}'} = 1.34\times10^6$ eV/cm	...
Optical	TO	$D^{0}_{\mathrm{T0},\mathbf{KK}'} = 3.41 \times 10^3$ eV/cm	$D^{0}_{\mathrm{T0},\mathbf{KK}'} = 2.48 \times 10^8$ eV/cm	...

resulting in stronger optical phonon scattering in α-graphyne as mentioned before. Compared with graphene and α-graphyne, the optical phonons scattering in γ-graphyne are weaker from the results of optical phonon DP constants.

In order to better understand the different phonon scattering mechanism in graphene and α-graphyne (the electronic structure with Dirac cones), we utilize an analytical expression of the electron scattering rate. Presently, the intra-valley scattering rate by acoustic mode λ (λ = LA and TA) is expressed as[52]

$$\frac{1}{\tau^1_{\mathbf{k}\lambda}} = \frac{\left(D^1_\lambda\right)^2 k_B T \varepsilon_{\mathbf{k}}}{4\hbar^3 \upsilon_F^2 \rho \upsilon_\lambda^2}, \tag{18}$$

here, ρ is the mass density (0.774×10^{-6} kg/m^2 for graphene, 0.381×10^{-6} kg/m^2 for α-graphyne), $\epsilon_{\mathbf{k}}$ is the electron energy and υ_F is the Fermi velocity near the Dirac cone. υ_λ denotes the sound velocity, which can be obtained by linear fitting of the acoustic phonon frequency $\omega_{\mathbf{q}\lambda}$ with respect to the phonon wavevector $\mathbf{q}$ in the long-wavelength limit ($\omega_{\mathbf{q}\lambda} = \upsilon_\lambda|\mathbf{q}|$). We take the value of $\upsilon_{\mathrm{LA}} = 21.70 \times 10^3$ m/s, $\upsilon_{\mathrm{TA}} = 13.88 \times 10^3$ m/s for graphene, and $\upsilon_{\mathrm{LA}} = 16.0 \times 10^3$ m/s, $\upsilon_{\mathrm{TA}} = 5.21 \times 10^3$ m/s for α-graphyne. The index 1 in the scattering time $\tau^1_{\mathbf{k}\lambda}$ and DP constant D^1_λ means first-order. Similarly, the rate of optical phonon scattering (both intra- and inter-valley transitions) as well as the inter-valley acoustic phonon scattering is expressed as[53]

$$\frac{1}{\tau^0_{\mathbf{k}\lambda}} = \frac{\left(D^0_\lambda\right)^2}{\rho\omega_{\mathbf{q}\lambda}(\hbar\upsilon_F)^2}[(\varepsilon_{\mathbf{k}} - \hbar\omega_{\mathbf{q}\lambda})(n_{\mathbf{q}\lambda}+1)\Theta(\varepsilon_{\mathbf{k}} - \hbar\omega_{\mathbf{q}\lambda}) + (\varepsilon_{\mathbf{k}} + \hbar\omega_{\mathbf{q}\lambda})n_{\mathbf{q}\lambda}], \tag{19}$$

where $\Theta(x)$ is the Heaviside step function and $n_{\mathbf{q}\lambda}$ is the Bose-Einstein distribution function of phonon. The index 0 in the scattering time $\tau^0_{\mathbf{k}\lambda}$ and DP constant D^0_λ means the zeroth-order scattering. In the case of inter-valley scattering via acoustic and optical phonon modes, $\hbar\omega_{\mathbf{q}\lambda}$ takes the respective phonon energy at the zone-edge **K**-point corresponding to electron transition $\mathbf{K} \rightarrow \mathbf{K}'$. The specific values of phonon energies used in Eq. (19) can be found in Table III. Fig. 9(a) shows the electron scattering times of graphene and α-graphyne as a function of the electron energy in the **K**-valley at room temperature. Notably, we define the overall zeroth-order and first-order scattering rates as

$$\frac{1}{\tau^0} = \frac{1}{\tau_{LA,\mathbf{KK}'}} + \frac{1}{\tau_{TA,\mathbf{KK}'}} + \frac{1}{\tau_{LO,\mathbf{KK}}} + \frac{1}{\tau_{LO,\mathbf{KK}'}} + \frac{1}{\tau_{TO,\mathbf{KK}}} + \frac{1}{\tau_{TO,\mathbf{KK}'}}, \tag{20}$$

and

$$\frac{1}{\tau^1} = \frac{1}{\tau_{LA,\mathbf{KK}}} + \frac{1}{\tau_{TA,\mathbf{KK}}}. \tag{21}$$

As can be seen from Fig. 9(a), at low electronic energy, the intra-valley acoustic phonon mode displays the lowest scattering time consistent with its large coupling strength in both graphene and α-graphyne. Meanwhile, compared to graphene, α-graphyne exhibits lower first-order scattering time due to its stronger acoustic phonon scattering. It is clear from the figure that the role of optical phonon scattering must be taken into accounts even at low electron energies, due to their significant coupling strength, especially for graphene. The discontinuities or steps in the curves of the zeroth-order scattering time represent either the onset of optical phonon emission or inter-valley scattering. For instance, the abrupt decrease in the curve of the zeroth-order scattering time in α-graphyne at ~248 meV can be attributed to the emission of a TO phonon of $\mathbf{q} = \mathbf{K}$ according to Table III. Similarly, the discontinuity for graphene is at ~159 meV, due to the inter-valley LO phonon scattering with $\mathbf{q} = \mathbf{K}$.

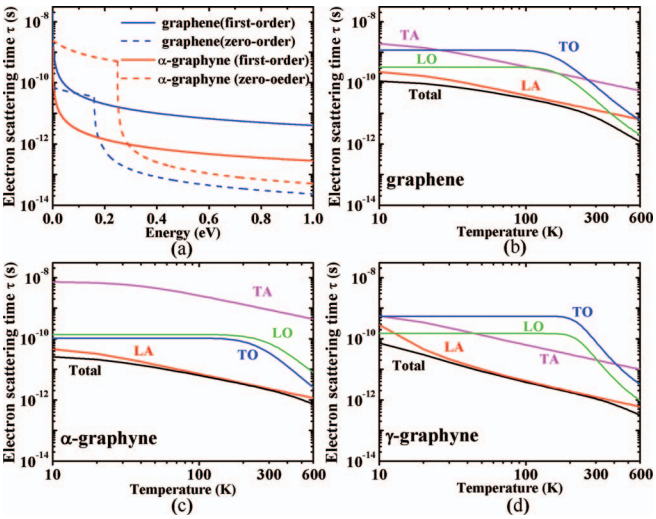

FIG. 9. (a) Zeroth-order and first-order scattering times as a function of electron energy at room temperature for graphene (blue lines) and α-graphyne, respectively. The solid lines are for first-order and dotted lines are for zeroth-order. (b)–(d) The scattering times of an electron at the CB minimum for different e-ph mode couplings as a function of temperature for graphene, α-graphyne, and γ-graphyne, according to Eq. (5) (black lines for total, red lines for LA, pink lines for TA, green lines for LO, and blue lines for TO).

D. Charge carrier transport

With the electron energies, phonon energies, and e-ph coupling matrix elements of graphene, α-graphyne and γ-graphyne from the first-principles calculations, the electron scattering times can be extracted according to Eq. (5). The scattering times of an electron at the CB minimum for LA, TA, LO, and TO modes as a function of temperature are shown in Figs. 9(b)–9(d). The total scattering times are also plotted in these figures based on Matthiessen's rule. Conveniently, the electron (hole) scattering time with **k** at the CB minimum (valence band VB maximum) for these three systems at room temperature are summarized in Table VI. It indicates that (i) the carrier scattering time (e.g., electron) by LA phonon scattering times at room temperature for both graphene (12.78 ps) and α-graphyne (2.33 ps) are in good agreement with our previous works based on the DP theory (13.94 ps for graphene, 2.83 ps for α-graphyne);[15] (ii) the LA phonon scattering is the main scattering mechanism over a large range of temperature for these systems, even at room temperature, resulting from its strong coupling strength; (iii) At low temperatures, due to the few excitation of

TABLE VI. The scattering times (in ps) for electrons at CB minimum and holes at VB maximum with different e-ph coupling mechanisms in graphene, α-graphyne, and γ-graphyne at room temperature. The total scattering times are also obtained with Matthiessen's rule.

	Graphene		α-graphyne		γ-graphyne	
Phonon mode	Hole	Electron	Hole	Electron	Hole	Electron
LA	14.28	12.78	2.17	2.33	0.56	1.25
TA	161.32	111.46	711.64	882.80	16.30	20.27
LO	27.78	26.43	68.74	70.06	17.07	22.61
TO	74.98	76.02	33.57	34.29	59.19	79.78
Total	7.97	7.24	1.97	2.11	0.52	1.10

TABLE VII. The electron and hole mobilties with different e-ph coupling mechanisms for graphene, α-graphyne, and γ-graphyne at room temperature. The total mobilites are also obtained with Matthiessen's rule. The unit is 10^4 $cm^2\ V^{-1}\ s^{-1}$.

	Graphene		α-graphyne		γ-graphyne	
Phonon mode	Hole	Electron	Hole	Electron	Hole	Electron
LA	41.38	34.12	0.99	1.07	0.39	2.42
TA	591.81	304.75	314.66	380.06	7.30	13.04
LO	82.43	78.22	73.41	75.12	7.61	10.05
TO	218.06	222.53	59.16	59.70	27.82	37.81
Total	23.49	20.05	0.96	1.03	0.35	1.62

high-frequency optical phonons, the optical phonon scattering is suppressed and the electron scattering time by optical phonon scattering remains almost unchanged with increasing temperature; (iv) the optical phonon scattering should not be neglected at high temperatures, due to the increasing number of optical phonons and significant coupling strength, especially for graphene, where the scattering time curves of LA and LO exhibit a crossover at around 400 K.

From the above analysis of e-ph couplings and electron scattering times, it is elucidated that the LA phonon scattering is the dominant mechanism over a wide range of temperature. According to Eq. (6), we estimate the electron mobility by LA phonon scattering for graphene, α-graphyne, and γ-graphyne, as a function of temperature (Fig. 10). The electron mobility limited by LA phonon scattering displays the $\mu \propto T^{-1}$ temperature dependence, which displays typical 2D transport behavior with acoustic phonon scattering above the Bloch-Grűneisen temperature.[54] Compared to graphene, the mobility of both α-graphyne and γ-graphyne is found to be one order of magnitude lower, resulting from the stronger e-ph coupling strength with LA phonon. Table VII shows the electron and hole mobilities limited by different phonon scattering mechanisms for graphene, α-graphyne, and γ-graphyne at room temperature. The overall mobilities are also obtained based on Matthiessen's rule. From the table, we see that scattering by LA phonon is expected to be the most important limiting factor for the mobility of 2D carbon materials investigated here. Actually, the electron velocity with energy $k_B T$ at

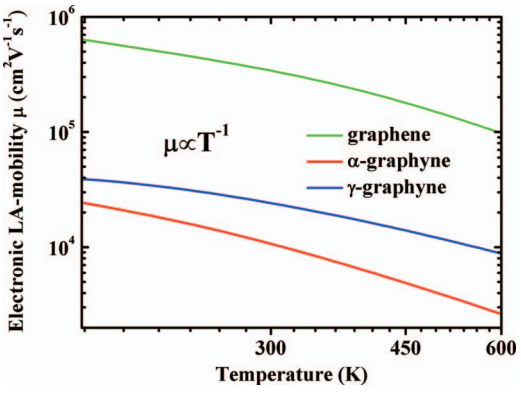

FIG. 10. Electron mobility for LA phonon scattering as a function of temperature for graphene (green line), α-graphyne (red line), and γ-graphyne (blue line). The mobility with the $\mu\alpha T^{-1}$ temperature dependence is shown.

300 K is about 10^5 m/s. The corresponding de Broglie wavelength is 7 nm, which is much larger than the lattice constant, thus the electron is scattered mainly by the acoustic phonons. However, LO phonon scattering also plays an important role to limit the carrier scattering times and mobilities at room temperature for graphene, due to its strong coupling strength. The electron mobilites for both α-graphyne and γ-graphyne at room temperature achieve the order of 10^4 $cm^2\ V^{-1}\ s^{-1}$, close to our previous results with the DP theory.[15]

IV. CONCLUSIONS

We have performed first-principles calculations to investigate momentum-dependent e-ph coupling and intrinsic carrier transport properties in two novel 2D carbon materials: α-graphyne and γ-graphyne. The e-ph coupling and charge carrier transport in graphene were also studied for comparison. In order to obtain refined electron energies, phonon energies, and e-ph coupling matrix elements for mobility calculation, the Wannier-interpolation method was applied. Due to the localization of the Hamiltonian, the dynamical matrix, and the e-ph coupling matrix in Wannier space, the interpolation based on truncated space are accurate. Our results elucidated that the main scattering mechanism in these 2D carbon materials is LA phonon, while the optical phonon could play some roles at high temperatures and even at low electron energies, especially for graphene. The predicted intrinsic mobilities of α-graphyne and γ-graphyne are both a few 10^4 $cm^2\ V^{-1}\ s^{-1}$ at room temperature. The lower mobility for α-graphyne and γ-graphyne compared to graphene is due to the stronger LA phonon scattering in both systems.

ACKNOWLEDGMENTS

This work is supported by the National Natural Science Foundation of China (Grant Nos. 21290190, 91333202, and 21273124) and the Ministry of Science and Technology of China (Grant Nos. 2011CB932304, 2011CB808405, and 2013CB933503).

[1]. S. Das Sarma, S. Adam, E. H. Hwang, and E. Rossi, Rev. Mod. Phys. **83**, 407 (2011).
[2]A. K. Geim, Science **324**, 1530 (2009).
[3]K. S. Novoselov, A. K. Geim, S. V. Morozov, D. Jiang, M. I. Katsnelson, I. V. Grigorieva, S. V. Dubonos, and A. A. Firsov, Nature **438**, 197 (2005).
[4]Y. Zhang, Y.-W. Tan, H. L. Stormer, and P. Kim, Nature **438**, 201 (2005).

[5]A. N. Enyashin and A. L. Ivanovskii, Phys. Status Solidi B **248**, 1879 (2011).
[6]Y. Liu, G. Wang, Q. Huang, L. Guo, and X. Chen, Phys. Rev. Lett. **108**, 225505 (2012).
[7]C. Su, H. Jiang, and J. Feng, Phys. Rev. B **87**, 075453 (2013).
[8]D. Malko, C. Neiss, F. Viñes, and A. Görling, Phys. Rev. Lett. **108**, 086804 (2012).
[9]B. G. Kim and H. J. Choi, Phys. Rev. B **86**, 115435 (2012).
[10]R. Baughman, H. Eckhardt, and M. Kertesz, J. Chem. Phys. **87**, 6687 (1987).
[11]M. Long, L. Tang, D. Wang, Y. Li, and Z. Shuai, ACS Nano **5**, 2593 (2011).
[12]L. Pan, L. Zhang, B. Song, S. Du, and H.-J. Gao, Appl. Phys. Lett. **98**, 173102 (2011).
[13]Q. Zheng, G. Luo, Q. Liu, R. Quhe, J. Zheng, K. Tang, Z. Gao, S. Nagase, and J. Lu, Nanoscale **4**, 3990 (2012).
[14]G. Li, Y. Li, H. Liu, Y. Guo, Y. Li, and D. Zhu, Chem. Commun. **46**, 3256 (2010).
[15]J. Chen, J. Xi, D. Wang, and Z. Shuai, J. Phys. Chem. Lett. **4**, 1443 (2013).
[16]J. Xi, M. Long, L. Tang, D. Wang, and Z. Shuai, Nanoscale **4**, 4348 (2012).
[17]M. Long, L. Tang, D. Wang, L. Wang, and Z. Shuai, J. Am. Chem. Soc. **131**, 17728 (2009).
[18]L. Tang, M. Long, D. Wang, and Z. Shuai, Sci. China Ser. B: Chem. **52**, 1646 (2009).
[19]J. Bardeen and W. Shockley, Phys. Rev. **80**, 72 (1950).
[20]K. I. Bolotin, K. J. Sikes, J. Hone, H. L. Stormer, and P. Kim, Phys. Rev. Lett. **101**, 096802 (2008).
[21]J.-H. Chen, C. Jang, M. Ishigami, S. Xiao, W. Cullen, E. Williams, and M. Fuhrer, Solid State Commun. **149**, 1080 (2009).
[22]X. Hong, A. Posadas, K. Zou, C. H. Ahn, and J. Zhu, Phys. Rev. Lett. **102**, 136808 (2009).
[23]V. Perebeinos and P. Avouris, "Current saturation and surface polar phonon scattering in graphene," preprint arXiv:0910.4665 (2009).
[24]K. M. Borysenko, J. T. Mullen, E. A. Barry, S. Paul, Y. G. Semenov, J. M. Zavada, M. B. Nardelli, and K. W. Kim, Phys. Rev. B **81**, 121412 (2010).
[25]K. Kaasbjerg, K. S. Thygesen, and K. W. Jacobsen, Phys. Rev. B **85**, 115317 (2012).
[26]K. M. Borysenko, J. T. Mullen, X. Li, Y. G. Semenov, J. M. Zavada, M. B. Nardelli, and K. W. Kim, Phys. Rev. B **83**, 161402 (2011).
[27]F. Giustino, M. L. Cohen, and S. G. Louie, Phys. Rev. B **76**, 165108 (2007).
[28]N. Vukmirović, C. Bruder, and V. M. Stojanović, Phys. Rev. Lett. **109**, 126407 (2012).
[29]M. Casula, M. Calandra, and F. Mauri, Phys. Rev. B **86**, 075445 (2012).
[30]S. Baroni, S. de Gironcoli, A. Dal Corso, and P. Giannozzi, Rev. Mod. Phys. **73**, 515 (2001).
[31]M. Wierzbowska, S. de Gironcoli, and P. Giannozzi, "Origins of low- and high-pressure discontinuities of T_c in niobium," preprint arXiv:cond-mat/0504077 (2005).
[32]G. Grimvall, *The Electron-Phonon Interaction in Metals, Selected Topics in Solid State Physics* (North-Holland, Amsterdam, 1981).
[33]J. W. Ziman, *Principles of the Theory of Solids* (Cambridge University Press, London, 1972).
[34]N. Marzari, A. A. Mostofi, J. R. Yates, I. Souza, and D. Vanderbilt, Rev. Mod. Phys. **84**, 1419 (2012).
[35]I. Souza, N. Marzari, and D. Vanderbilt, Phys. Rev. B **65**, 035109 (2001).
[36]G. Paolo *et al.*, J. Phys.: Condens. Matter **21**, 395502 (2009).
[37]H. J. Monkhorst and J. D. Pack, Phys. Rev. B **13**, 5188 (1976).
[38]J. Noffsinger, F. Giustino, B. D. Malone, C.-H. Park, S. G. Louie, and M. L. Cohen, Comput. Phys. Commun. **181**, 2140 (2010).
[39]A. A. Mostofi, J. R. Yates, Y.-S. Lee, I. Souza, D. Vanderbilt, and N. Marzari, Comput. Phys. Commun. **178**, 685 (2008).
[40]J. D. Cloizeaux, Phys. Rev. **135**, A698 (1964).
[41]G. Nenciu, Commun. Math. Phys. **91**, 81 (1983).
[42]J.-A. Yan, W. Y. Ruan, and M. Y. Chou, Phys. Rev. B **79**, 115443 (2009).
[43]S. Piscanec, M. Lazzeri, F. Mauri, A. C. Ferrari, and J. Robertson, Phys. Rev. Lett. **93**, 185503 (2004).
[44]Q. Peng, W. Ji, and S. De, Phys. Chem. Chem. Phys. **14**, 13385 (2012).
[45]V. O. Özçelik and S. Ciraci, J. Phys. Chem. C **117**, 2175 (2013).
[46]J. Kang, J. Li, F. Wu, S.-S. Li, and J.-B. Xia, J. Phys. Chem. C **115**, 20466 (2011).
[47]X.-M. Wang, D.-C. Mo, and S.-S. Lu, J. Chem. Phys. **138**, 204704 (2013).
[48]W. Kohn, Phys. Rev. Lett. **2**, 393 (1959).
[49]J.-A. Yan, R. Stein, D. M. Schaefer, X.-Q. Wang, and M. Y. Chou, Phys. Rev. B **88**, 121403 (2013).
[50]D. K. Ferry, *Semiconductor Transport* (Taylor and Francis, New York, 2000).
[51]K. Kaasbjerg, K. S. Thygesen, and K. W. Jacobsen, Phys. Rev. B **85**, 165440 (2012).
[52]E. H. Hwang and S. Das Sarma, Phys. Rev. B **77**, 115449 (2008).
[53]R. S. Shishir and D. K. Ferry, J. Phys.: Condens. Matter **21**, 344201 (2009).
[54]H. L. Stormer, L. N. Pfeiffer, K. W. Baldwin, and K. W. West, Phys. Rev. B **41**, 1278 (1990).